Journal of Quantitative Spectroscopy & Radiative Transfer 262 (2021) 107529

Contents lists available at ScienceDirect

Journal of Quantitative Spectroscopy & Radiative Transfer

journal homepage: www.elsevier.com/locate/jqsrt

Spectrum of beryllium dimer in ground $X^1\Sigma_g^+$ state

V.L. Derbov[a], G. Chuluunbaatar[b,c], A.A. Gusev[b,*], O. Chuluunbaatar[b,d], S.I. Vinitsky[b,c], A. Góźdź[e], P.M. Krassovitskiy[b,f], I. Filikhin[g], A.V. Mitin[h,i]

[a] N.G. Chernyshevsky Saratov National Research State University, Saratov, Russia
[b] Joint Institute for Nuclear Research, Dubna, Russia
[c] Peoples' Friendship University of Russia (RUDN University), 117198 Moscow, Russia
[d] Institute of Mathematics and Digital Technology, Mongolian Academy of Sciences, Ulaanbaatar, Mongolia
[e] Institute of Physics, University of M. Curie-Skłodowska, Lublin, Poland
[f] Institute of Nuclear Physics, Almaty, Kazakhstan
[g] Department of Mathematics and Physics,North Carolina Central University, Durham, NC 27707, USA
[h] Moscow Institute of Physics and Technology, 9 Institutskiy per., Dolgoprudny, Moscow Region, 141700, Russia
[i] Joint Institute for High Temperatures of RAS, Izhorskaya st. 13 Bd.2, 125412 Moscow, Russia

ARTICLE INFO

Article history:
Received 6 December 2020
Revised 19 January 2021
Accepted 19 January 2021
Available online 22 January 2021

Keywords:
Beryllium dimer
Spectrum of bound and metastable states
Eigenvalue and scattering problems
Finite element method

ABSTRACT

The calculations of the spectrum of vibrational-rotational bound states and new metastable states of the beryllium dimer in ground $X^1\Sigma_g^+$ state important for laser spectroscopy are presented. The problem is solved using the potential energy curves from [A.V. Mitin, Chem. Phys. Lett. 682, 30 (2017)] and [M. Lesiuk et al, Chem. Theory Comput. 15, 2470 (2019)], and the authors' software package that implements the iteration Newton method and the high-accuracy finite element method. The efficiency of the proposed approach is demonstrated by the upper and lower estimates of the spectrum of vibrational-rotational bound states and, for the first time, rotational-vibrational metastable states with complex-valued energy eigenvalues (with negative imaginary parts of the order of $(10^{-20} \div 6)$ cm^{-1}) in the beryllium dimer. The existence of these metastable states is confirmed by calculating the corresponding scattering states with real-values resonance energies.

1. Introduction

During the last decade, theoretical studies [1–6] have shown twelve vibrational bound states in the beryllium dimer, whereas 11 states were extracted from the experimental data of laser pump-probe spectroscopy (see Fig. 1 in Ref. [7]). Earlier [8] we started to study the vibration-rotation spectrum of the beryllium dimer. We solved the boundary value problem (BVP) for the second-order ordinary differential equation with potential energy curve (PEC) numerically tabulated on a non-uniform grid in a finite interval of the independent variable values [4]. To formulate the BVP on a semi-axis, the PEC should be continued beyond the finite interval using the additional information about the interaction of atoms comprising the diatomic molecule at large interatomic distances. The dominant term of the PEC at large distances is given by the van der Waals interaction, inversely proportional to the sixth power of the independent variable with the constant, determined from theory [9,10]. Proceeding in this way we faced a problem how to match the asymptotic expansion of the PEC with its tabulated numerical values (within the accuracy of their calculation) at a suitable sufficiently large distance and calculate correctly the required sets of bound and metastable states [11].

In the present paper we continue studying these problems. We recall the results of the spectrum of the vibrational-rotational bound states and present the improved calculations of the spectrum of the rotational-vibrational metastable states of the beryllium dimer having complex-valued eigenenergies. The existence of these metastable states is confirmed by calculation of the corresponding scattering states with real values of the resonance energies. High-precision theoretical *upper and lower estimates* are of significant importance for further experiments in laser spectroscopy of the beryllium dimer. It is also important for modeling of a near-surface diffusion of the beryllium dimers [12] in connection with the well-known multifunctional use of beryllium alloys in modern technologies of the electronic, space and nuclear industries [13], and, in particular, the ITER project [14]. The adaptation of technique for solving the above class of eigenvalue, metastable and scattering problems for the second order ordinary differential equations using the programs ODPEVP [15], KANTBP[16–18], and

* Corresponding author.
E-mail address: gooseff@jinr.ru (A.A. Gusev).

https://doi.org/10.1016/j.jqsrt.2021.107529
0022-4073/

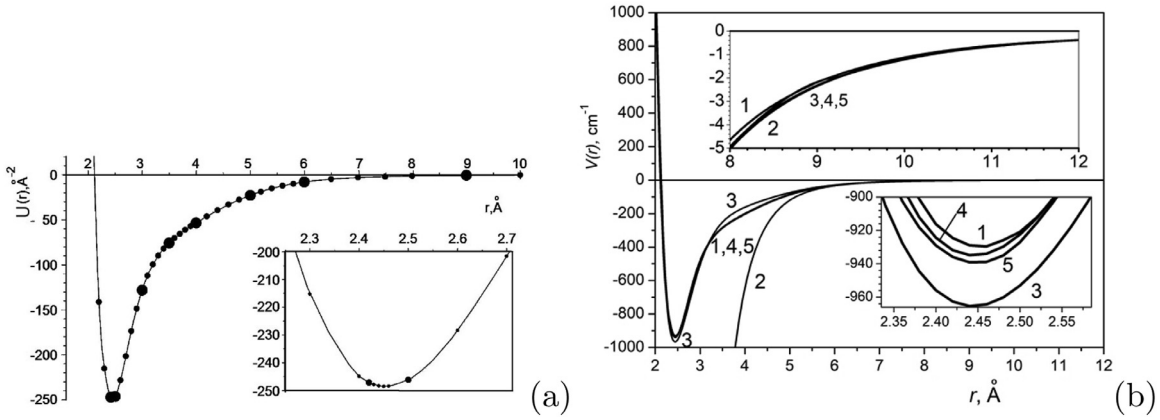

Fig. 1. (a) Potential $V(r)$ (Å^{-2}.) of the beryllium dimer as a function of r (Å) obtained by interpolating the tabulated values [4] (points in the subintervals, the boundaries of which are shown by larger-size circles) by fifth-order LIPs. (b) MEMO potential $V(r)$ (points and line 1 [4]), the asymptotic expansion $V_{\rm as}(r)$ of MEMO function (line 2, [9]), the analytical forms of the potential function $V_{an}(r)$ (line 3 [10] and line 4 [6] and line 5 [5]). r is given in Å, $\tilde{V}_*(r)$ in cm^{-1}.

KANTBP 5M[19], i.e., the upgraded version of KANTBP 4M [20], implementing the finite element method (FEM) [21,22] in Fortran and Maple, respectively, is also a subject of the present study.

The paper has the following structure. Section 2 describes the procedure of approximation of PEC and its extension on large interval by means of the matching procedure using Hermite interpolation polynomials (HIPs). In Section 3 we present the results of calculating the spectrum of vibrational-rotational bound states of the beryllium dimer. Section 4 demonstrates the calculation of the spectrum of rotational-vibrational metastable states with complex values of eigenenergy of the beryllium dimer. In section 5 we present examples of scattering states at resonance energies that confirm the existence of the typical metastable states under consideration. In Conclusion we discuss further applications of the elaborated method and results.

2. The potential energy curves and its extension on a large interval

In quantum chemical calculations, the PEC of interatomic interaction are presented in the form of numerical tables calculated with limited accuracy and defined on a nonuniform mesh of nodes in a finite domain of interatomic distance variation. However, for a number of diatomic molecules the asymptotic expressions for the PEC are calculated analytically for sufficiently large distances between the atoms. The Schrödinger equation for a diatomic molecule in the adiabatic approximation (in which the diagonal nonadiabatic correction is not taken into account), commonly referred to as Born–Oppenheimer (BO) approximation, has the form

$$\left(-\frac{\hbar^2}{2mDa\text{Å}^2}\left(\frac{1}{r^2}\frac{d}{dr}r^2\frac{d}{dr}\right)+V_L(r)-E\right)\Phi_L(r)=0, \qquad (1)$$

$$V_L(r)=V(r)+\frac{\hbar^2}{2mDa\text{Å}^2}\frac{L(L+1)}{r^2},$$

where L is the total angular momentum quantum number, $\hbar^2/(2Da)$=1.685762920·10^{-7} Å, the reduced mass of beryllium molecule is m=M/2=4.506, r is expressed in Å, Da = 9.10938356 · 10^{-31}kg= 931.494061MeV is the dalton (atomic mass unit) [23], E is the energy in cm^{-1} and $V(r)$ is PEC in cm^{-1} at $L=0$. The BVP for Eq. (1) was solved in the following units: the variable r is expressed in (Å), the PEC $U(r)=(2mDa\text{Å}^2/\hbar^2)V(r)$ in Å^{-2}, and the desired value of energy $\mathcal{E}$=$(2mDa\text{Å}^2/\hbar^2)E$ in Å^{-2}, i.e. E=$s_2\mathcal{E}$ cm^{-1} and $V(r)$=$s_2U(r)$ cm^{-1}, where $s_2=1/0.2672973729$ is the conversion factor from Å^{-2} to cm^{-1}.

In Ref. [4] the potential $V(r)$ (in cm^{-1}) (see Fig. 1) is given by the BO potential function marked as the modified expanded Morse oscillator (MEMO) tabular values $\{V^M(r_i)\}_{i=1}^{76}$ in interval $r\in[r_1=1.5, r_{76}=48]$Å. These tabular values were chosen to provide better approximation of the potential $V(r)$ by the fifth-order Lagrange interpolation polynomials (LIPs) of the variable r in subintervals $r\in[r_{5k-4}, r_{5k+1}]$, $k=1,\ldots,15$. Indeed, one can see that Fig. 1a displays a smooth approximation till $r_{49}=12$, where the approximate PEC coincides with and crosses the asymptotic potential $V_{\rm as}^{\rm BO}(r)=s_2U_{\rm as}^{\rm BO}(r)$ given analytically by the expansions [9]

$$U_{\rm as}^{\rm BO}(r)=s_1\tilde{V}_{\rm as}^{\rm BO}(r),\quad \tilde{V}_{\rm as}^{\rm BO}(r)=-\left(214Z^{-6}+10230Z^{-8}+504300Z^{-10}\right), \qquad (2)$$

where s_1 = 58664.99239 is the conversion factor from aue to Å^{-2}, $Z=r/s_3$ and s_3 = 0.52917 is Bohr radius in Å. This fact allows considering the interval $r\in[r_{\rm match}\geq 12,\infty)$ as possible for using the asymptotic potential $V_{\rm as}^{\rm BO}(r)$ at large r and executing conventional calculations based on tabular values of $V(r)$ in the finite interval $r\in[r_1, r{=}12]$ (see also [6]). However, the above MEMO tabular values have been calculated in the unusually larger interval $r\in[r_1, r{=}48]$ using special composite basis functions in different subintervals, taking into account both polarization and relativistic corrections by the Douglas-Kroll-Hess method [24–26], and the extrapolation to the infinite basis set [27] marked as DK-MRCI in the subinterval $r\in[r=12, r=48]$ [2].

We note that the MEMO tabular values for $r\in\{r_{41}=6.5,\ldots,r_{48}=11\}$ are smaller than the asymptotic ones by 5.5 ÷ 6%, for $r=r_{51}=14$ exceed the asymptotic ones by 8%, and beyond the interval $r\in[r_{40}=6.0,\ldots,r_{52}=15]$ the difference is more than 10%. Based on this fact, in Ref. [11] we considered three cases of approximation of this potential function in the extended interval marked by the key $K=-1$, -3 or -4.

Here we use only the key $K=-1$, the potential $V(r)$ in subintervals $r\in[r_{5k-4}, r_{5k+1}]$, $k=1,\ldots,9$ was approximated by the fifth-order Lagrange interpolation polynomials (LIPs) of the variable r in the interval $r\in[r_1, r_{46}=14]$. In subinterval $r\in[r_e=r_{46}=9, r_{\rm match}=14]$ we consider the approximation of the potential $V(r)$ by the fourth-order HIPs using the values of the potential $V(r)$ at the points $r=\{r_e=r_{46}=9, r_{47}=10, r_{48}=11\}$ and the values of the asymptotic potential $V_{\rm as}(r)$ and its derivative $dV_{\rm as}(r)/dr$ at the point $r=r_{\rm match}=14$. In the $r\in[r_{\rm match}=14,\infty)$ the potential $V(r)$ is approximated by the asymptotic expansion (2). This approximation has been accepted in our paper [8].

In Ref. [6] the potential $V(r)$ (in cm^{-1}) (see Fig. 1) is given by the BO potential function plus relativistic potential function

Table 1
Comparison of the vibrational spectra $E_{v=0,L=0} - E_{vL=0}$ (in cm^{-1}) for the $X^1\Sigma_g^+$ state of the beryllium dimer: the eigenvalues of vibrational energy $-E_{vL=0}$ (in cm^{-1}) of the beryllium dimer calculated by the KANTBP 4M [20] and ODPEVP [15] programs implementing FEM (FEM(MEMO)) using FEM approximation of PEC MEMO from [4] and FEM(STO) using FEM approximation of PEC STO from Lesiuk et al. [6], theoretical (EMO) and experimental (Exp) results [7], combined ab initio [2] and EMO calculations tabulated as modified EMO (MEMO) [4], symmetry-adapted perturbation theory (SAPT) [1], the Morse-long range (MLR) function and Chebyshev polynomial expansion (CPE) [5], the ab initio potential CV+F+R calculated in [3] and Slater-type orbitals (STO) [6]; D_e is the well depth and $D_0 = E_{v=0,L=0}$ is the dissociation energy in cm^{-1}, r_e is the equilibrium internuclear distance in Å, rms is root-mean-square discrepancy between the theoretical and experimental data.

v	STO	FEM STO	FEM MEMO	MEMO	EMO	Exp	SAPT	MLR CPE	CV+ F+R
r_e	2.4344	2.447	2.4534	2.4534	2.4535	2.4536	2.443	2.445	2.4436
D_e	934.6	934.4	929.804	929.74	929.74	929.7±2	938.7	934.8	935±10
D_0	807.7	807.7	806.07	806.48	806.5	807.4	812.4	808.15	808.3
1	223.4	223.5	222.50	222.16	222.7	222.6	222.3	222.91	222.7
2	400.1	398.2	397.34	397.6	397.8	397.1	397.6	397.41	396.8
3	517.3	519.3	517.71	517.87	518.2	518.1	520.3	518.41	517.8
4	595.1	595.7	594.89	595.06	595.4	594.8	597.9	595.08	594.7
5	651.7	652.2	651.91	652.10	652.4	651.5	655.1	651.79	651.6
6	698.7	699.3	698.92	699.14	699.4	698.8	702.6	699.03	698.9
7	738.0	738.1	737.72	737.97	738.2	737.7	741.7	737.97	738.0
8	769.3	768.6	768.27	768.56	768.8	768.2	772.4	768.50	768.6
9	790.1	790.1	789.74	790.05	790.7	789.9	794.3	790.17	790.4
10	802.6	802.6	801.66	802.08	803.4	802.6	807.1	802.83	803.1
11	807.5	807.2	805.74	806.21			811.9	807.53	807.9
rms	1.0	0.7	0.4	0.4	0.6		3.4	0.3	0.3

marked as STO tabular values $\{V^M(Z_i)\}_{i=1}^{28}$ in interval $Z \in [Z_1 = 3.75, Z_{28} = 25]$ a.u. which corresponds to $r \in [r_1 = 1.9843, r_{28} = 13.229]$ Å. One can see that these tabular values were chosen to provide the best approximation of the potential $V(r)$ by the fourth-order LIPs of the variable r in subintervals $r \in [r_{4k-3}, r_{4k+1}]$, $k = 1, \ldots, 6$. On interval $Z \in [Z_{25}, Z_{\rm match} = 27.5]$ a.u. we consider the approximation of the potential $V(r)$ by the fifth-order HIP using the values of the potential $V(Z)$ at the points $r = \{r_{25} = 17.5, r_{26} = 20.0, r_{27} = 22.5, r_{28} = 25.0\}$a.u. and the values of the asymptotic potential $V_{\rm as}(r)$ and its derivative $dV_{\rm as}(V)/dZ = s_3 dV_{\rm as}(r)/dr$ at the point $Z = Z_{\rm match} = 27.5$ a.u.. In the $r \in [r_{\rm match} = 14.552, \infty)$ Å the potential $V_{\rm as}(r) = s_2 U_{\rm as}(r)$ is approximated by the asymptotic expansion

$$U_{\rm as}(r) = s_1 \tilde{V}_{\rm as}(r), \quad \tilde{V}_{\rm as}(r) = \tilde{V}_{\rm as}^{\rm BO}(r) + \tilde{V}_{\rm as}^{\rm rel}(r), \tilde{V}_{\rm as}^{\rm rel}(r) = - \left(1.839 \cdot 10^{-4} Z^{-4} + 0.11944 Z^{-6} + 19.582 Z^{-8} - 1323.5 Z^{-10}\right), \quad (3)$$

where $\tilde{V}_{\rm as}^{\rm BO}(r)$ and $\tilde{V}_{\rm as}^{\rm rel}(r)$ are given by (2) and [6], respectively. Using similar behaviour MEMO and STO potential functions on the interval $r \in [12, 14]$Å one can use also (3) for matching MEMO potential in interval $r \in [14, \infty)$Å, because of it was calculated by DK-MRCI method.

For comparison we show in Fig. 1 the potential function $V(r)$, its asymptotic expansion $V_{\rm as}(r)$ and the analytical potential functions $V_{an}(r)$ in a.u. (converted into cm^{-1}), proposed in Ref. [10]. The MEMO potential function $V(r)$ has a minimum $-D_e(\text{FEM}) = V(R_e) = -929.804$ cm^{-1} at the equilibrium point $R_e = 2.4534$ Å, which is higher than the analytical potential function $V_{an}(r)$ in the vicinity of this point, $-D_e(\text{Sheng}) = V_{\rm an}(R_e) = -948.3$ cm^{-1}. On the contrary, in the interval $r \in (3.2, 6.1)$ the analytical potential function $V_{\rm an}(r)$ is greater than $V(r)$. For $r \in (2.3, 12)$ the MEMO potential slightly exceeds the STO one, which, in turn, is a bit higher than the MLR&CPE potential. Thus, using the accepted approximation with the key $K = -1$ we have the potential function $V(r)$ in the analytical form in interval $r \in (1.9, 14)$ and its smooth continuation at $r \geq 14$ by means of the asymptotic expression (2).

The MAPLE and FORTRAN programs of approximation of the MEMO [4] and STO [6] potential functions $V_L(r)$ are given in the supplementary material.

3. Bound states of the beryllium dimer

For calculation of the vibrational-rotational spectrum of the real-valued eigenenergies E_{vL} and corresponding eigenfunctions $\Phi_{vL}(r)$ of the bound states of the beryllium dimer we solved the BVP for Eq. (1) using the FEM programs KANTBP 4M and ODPEVP on the finite element mesh $\Omega_1 = \{$ 1.90, 1.95, 2.00, 2.07, 2.15, 2.22, 2.30, 2.36, 2.42, 2.50 (0.1) 4 (0.2) 6 (0.5) 14 (2) 44$\}$ with the second-type or Neumann boundary conditions (BCs) on the boundary points of the mesh. In each of the subintervals (except the last one) the potential $V(r)$ was approximated by a LIP of the fifth order. In the BVP solution at all finite elements of the mesh the local functions were represented by fifth-order HIPs.

Table 1 presents the results of using FEM programs KANTBP 4M and ODPEVP to calculate 12 energy eigenvalues of the beryllium dimer. It shows the eigenvalues calculated with the ab initio modified expanded Morse oscillator (MEMO) potential function [4] and the corresponding FEM approximation. In contrast to the original EMO function, which was used to describe the experimental (Exp) vibrational levels [7], it has not only the correct dissociation energy, but also describes all twelve vibrational energy levels with the RMS error less than 0.4 cm^{-1}. The table also shows the results of recent calculation using the Morse long-range (MLR) function and Chebyshev polynomial expansion (CPE) alongside with the EMO potential function [5], and CV+F+R potential function [3] discussed early in [2]. Similar results were obtained by Lesiuk et al. [6]. Their PEC lie below the MEMO one and also include the correct long-range behavior displayed in Fig. 1. As a consequence, one can see from the Table 1, that the corresponding results provide *a lower estimate* whereas FEM and MEMO results give *an upper estimate* for the discrete spectrum of the beryllium dimer at both $L = 0$ and $L > 0$. One can see also that the FEM (STO) eigenenergies calculated by using the above mentioned FEM approximation of the tabulated PEC STO gives smaller RMS error 0.7 cm^{-1} in comparison with RMS error 1.0 cm^{-1} of the STO eigenenergies calculated by using the analytical fit PEC STO [6].

The potential functions FEM (MEMO) and FEM (STO) $V_L(r)$ from $L = 0$ to $L = 36$ support $37 + 33 + 30 + 28 + 26 + 24 + 21 + 18 + 14 + 11 + 7 + 3 = 252$ and $37 + 33 + 30 + 28 + 26 + 24 + 21 + 18 +$

Table 2
vibrational-rotational bound states $-E_{vL}$ (in cm^{-1}) of the beryllium dimer. For each L in upper line MEMO and in lower line STO with relativistic corrections.

L	$v=0$	1	2	3	4	5	6	7	8	9	10	11
0	806.0	583.5	408.7	288.3	211.1	154.1	107.1	68.3	37.8	16.3	4.4	0.3
0	807.7	584.1	409.4	288.3	211.9	155.4	108.3	69.5	39.0	17.5	5.0	0.4
1	804.8	582.4	407.7	287.5	210.4	153.5	106.6	67.8	37.4	16.0	4.2	0.2
1	806.5	583.0	408.4	287.5	211.2	154.8	107.7	69.0	38.6	17.2	4.8	0.3
2	802.4	580.1	405.7	285.8	209.0	152.3	105.5	66.9	36.6	15.4	3.8	0.1
2	804.0	580.8	406.4	285.8	209.8	153.5	106.7	68.1	37.8	16.6	4.4	0.1
3	798.7	576.7	402.6	283.2	206.9	150.4	103.8	65.5	35.4	14.5	3.2	
3	800.4	577.4	403.5	283.3	207.7	151.7	105.1	66.7	36.7	15.7	3.8	
4	793.9	572.2	398.6	279.8	204.1	148.0	101.7	63.6	33.8	13.3	2.4	
4	795.5	573.0	399.5	279.9	204.9	149.3	102.9	64.8	35.1	14.5	3.0	
5	787.8	566.5	393.6	275.6	200.5	144.9	99.0	61.2	31.8	11.8	1.5	
5	789.5	567.4	394.5	275.8	201.5	146.3	100.2	62.5	33.2	13.0	2.1	
6	780.5	559.7	387.5	270.6	196.3	141.2	95.7	58.4	29.5	10.0	0.5	
6	782.2	560.7	388.6	270.8	197.3	142.6	97.0	59.7	30.9	11.2	1.0	
7	772.1	551.8	380.5	264.7	191.4	137.0	92.0	55.2	26.8	8.1		
7	773.7	552.9	381.7	265.0	192.5	138.4	93.3	56.5	28.2	9.2		
8	762.4	542.8	372.5	258.0	185.9	132.1	87.7	51.5	23.8	5.9		
8	764.1	544.0	373.8	258.4	187.0	133.6	89.1	52.9	25.2	7.0		
9	751.5	532.7	363.5	250.5	179.7	126.7	83.0	47.4	20.5	3.5		
9	753.2	534.0	364.9	251.0	180.9	128.3	84.4	48.8	21.9	4.6		
10	739.4	521.4	353.6	242.2	172.8	120.7	77.7	42.9	16.8	1.0		
10	741.1	522.9	355.1	242.8	174.2	122.4	79.2	44.3	18.3	2.0		
11	726.2	509.1	342.6	233.2	165.3	114.2	72.0	38.0	12.9			
11	727.9	510.7	344.4	233.9	166.8	115.9	73.6	39.5	14.4			
12	711.7	495.6	330.8	223.4	157.2	107.1	65.8	32.8	8.7			
12	713.4	497.4	332.7	224.3	158.8	108.9	67.4	34.3	10.2			
13	696.0	481.1	318.0	212.9	148.5	99.5	59.2	27.1	4.4			
13	697.8	483.1	320.1	213.9	150.2	101.4	60.9	28.7	5.9			
14	679.2	465.5	304.3	201.7	139.2	91.4	52.2	21.2				
14	681.0	467.7	306.6	202.8	141.0	93.4	53.9	22.9	1.4			
15	661.2	448.8	289.7	189.8	129.3	82.8	44.7	15.0				
15	663.0	451.2	292.2	191.1	131.3	84.8	46.5	16.7				
16	642.1	431.0	274.2	177.3	118.9	73.8	36.9	8.5				
16	643.8	433.7	276.9	178.7	121.1	75.9	38.8	10.3				
17	621.8	412.2	257.9	164.2	108.0	64.3	28.7	1.9				
17	623.5	415.1	260.8	165.8	110.3	66.5	30.7	3.7				
18	600.3	392.4	240.7	150.4	96.6	54.4	20.3					
18	602.1	395.5	243.8	152.2	99.0	56.6	22.3					

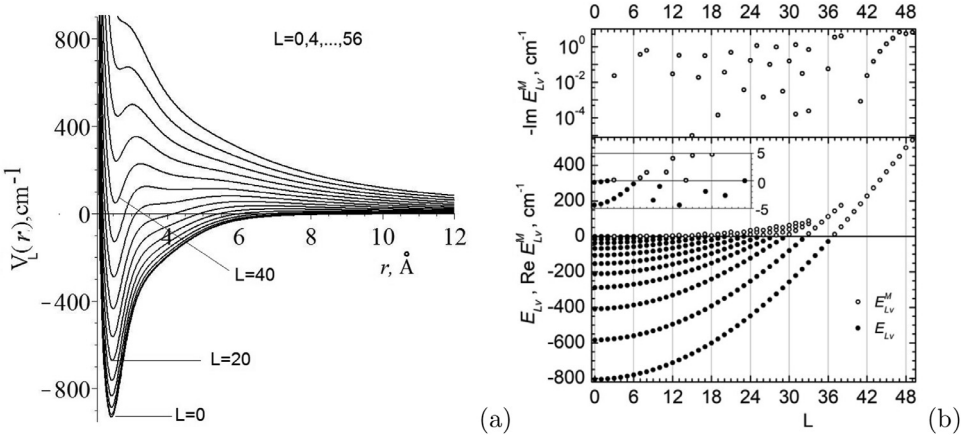

Fig. 2. (a) Potential functions $V_L(r)$ at $L = 0, 4, 8, \ldots, 56$. (b) Eigenenergies E_{vL} of vibrational-rotational bound states (lower panel) and real part $\Re E^M_{Lv}$ (lower panel) and imaginary part $-\Im E^M_{Lv}$ with negative sign (upper panel) of complex eigenenergies $E^M_{Lv} = \Re E^M_{Lv} + i\Im E^M_{Lv}$ of rotational-vibrational metastable states. $V_L(r)$ at $L = 0, 1, \ldots, 36$ and at $L = 0, 4, 8, \ldots, 56$.

$15 + 11 + 7 + 3 = 253$ vibrational-rotational energy levels $-E_{vL}$, respectively, presented in Table 2 and 3. Note, the bound state with energy $E_{L=14,v=8} = -1.44$ for PEC STO corresponds to the sharp metastable state for MEMO PEC with complex energy $E^M_{L=14,v=8} = 0.083 - \imath 3 \cdot 10^{-29}$. Fig. 2b shows also the rotational-vibrational spectrum $E_{vL} \equiv E_{Lv}$ (in cm^{-1}) of Be_2 vs L. These functions $\tilde{V}_L(r)$ are displayed in Fig. 2a at $L = 0, \ldots, 36$ with the step 4. One can see that the potential $V_L(r)$ at $L = 0$, $L = 1$ and $L = 2$ supports 12 vibrational energy levels. Note that the bound states are supported by the potentials $V_L(r)$ at $L = 0, 1, \ldots, 36$ (see Tables 2, 3 and Fig. 2a), while the metastable states are supported by the potentials $V_L(r)$ at $L = 3, 7, 8, 11, 12, 14, 15, 16, 18, 19, 20, 21, 22, 23, 24, 25, 26, 27, 28, 29, 30, 31, 32, 33, 34, 35, 36, 37, 38, 39, 40, 41, 42, 43, 44, 45, 46, 47, 48, 49$ (see Tables 4 and 6, and Fig. 2a).

Table 3
vibrational-rotational bound states $-E_{vL}$ (in cm^{-1}) of the beryllium dimer. For each L in upper line MEMO and in lower line STO with relativistic corrections. Continuation of Table 2.

L	$v=0$	1	2	3	4	5	6	7	8	9	10	11
19	577.7	371.5	222.8	136.2	84.8	44.1	11.5					
19	579.4	374.9	226.0	138.2	87.3	46.4	13.6					
20	553.9	349.7	204.0	121.5	72.5	33.5	2.6					
20	555.7	353.3	207.5	123.7	75.2	35.9	4.8					
21	529.1	326.8	184.6	106.3	59.8	22.5						
21	530.8	330.7	188.2	108.7	62.6	25.0						
22	503.1	303.0	164.4	90.8	46.8	11.4						
22	504.9	307.2	168.2	93.4	49.7	13.9						
23	476.0	278.2	143.6	74.9	33.4	0.01						
23	477.8	282.7	147.6	77.8	36.4	2.5						
24	447.8	252.5	122.3	58.8	19.8							
24	449.6	257.2	126.4	61.9	22.9							
25	418.5	225.9	100.4	42.5	5.9							
25	420.3	230.9	104.7	45.8	9.1							
26	388.2	198.4	78.2	26.0								
26	390.0	203.7	82.5	29.6								
27	356.7	170.1	55.7	9.5								
27	358.6	175.6	60.1	13.3								
28	324.3	140.9	33.1									
28	326.1	146.7	37.5									
29	290.8	111.0	10.7									
29	292.7	117.0	14.9									
30	256.3	80.4										
30	258.2	86.6										
31	220.8	49.1										
31	222.7	55.6										
32	184.4	17.2										
32	186.3	23.9										
33	146.9											
33	148.9											
34	108.6											
34	110.6											
35	69.3											
35	71.4											
36	29.2											
36	31.3											

Table 4
The rotational-vibrational metastable states $E^M_{Lv} = \Re E^M_{Lv} + \imath \Im E^M_{Lv}$ (in cm^{-1}) of Be_2, where "eps" means that $-10^{-5} < \Im E^M_{Lv} < 0$ (in cm^{-1}). From left to right MEMO and STO with relativistic corrections. $V_L^{\min}$ and $V_L^{\max}$ are minimal and maximum values of potentials $V_L(r)$ (in cm^{-1}) at different values L of the total angular momentum.

L	v	MEMO		STO		MEMO		STO	
		$V_L^{\min}$	$V_L^{\max}$	$V_L^{\min}$	$V_L^{\max}$	$\Re E$	$-\Im E$	$\Re E$	$-\Im E$
0		−929.74	0.00	−934.39	0.00				
1		−928.49	0.01	−933.15	0.03				
2		−926.00	0.04	−930.66	0.10				
3	11	−922.26	0.12	−926.92	0.21	0.092	0.014		
4		−917.27	0.22	−921.93	0.35				
5		−911.04	0.42	−915.70	0.52				
6		−903.59	0.71	−908.22	0.74				
7	10	−894.94	1.11	−899.49	1.09	0.504	5.5e-4	0.972	5.6e-3
8	10	−885.05	1.62	−889.52	1.57	1.508	0.078	2.315	0.149
9	10	−873.92	2.24	−878.30	2.18			3.781	0.499
10		−861.56	3.00	−865.92	2.92				
11	9	−847.96	3.92	−852.32	3.92	1.554	eps	0.783	eps
12	9	−833.12	5.02	−837.49	5.04	4.050	0.031	3.592	1.e-3
13	9	−817.04	6.27	−821.41	6.27			6.371	0.543
14	8	−799.73	7.73	−804.10	7.64	0.083	eps		
14	9	−799.73	7.73	−804.10	7.64			9.121	0.295
15	8	−781.19	9.39	−785.56	9.18	4.605	1.e-5	3.141	eps
15	9	−781.19	9.39	−785.56	9.18			11.957	0.7940
16	8	−761.44	11.26	−765.77	10.94	8.992	0.018	7.705	5.0e-4
17	8	−740.59	13.34	−744.92	12.94	13.016	0.314	12.09	0.032
18	7	−718.51	15.66	−722.84	15.19	4.788	eps	2.917	eps
18	8	−718.51	15.66	−722.84	15.19			16.16	0.2586
19	7	−695.21	18.22	−699.54	17.69	11.517	1.4e-4	9.637	eps
20	6	−670.68	21.05	−675.01	20.44	17.991	0.036	16.21	2.2e-3
21	6	−644.93	24.15	−649.25	23.45	6.403	eps	4.200	eps
21	7	−644.93	24.15	−649.25	23.45	23.915	0.482	22.33	0.090
22	6	−618.07	27.51	−622.46	26.73	15.497	eps	13.26	eps
23	5	−590.08	31.24	−594.48	30.30	24.444	3.7e-3	22.220	2.5e-4

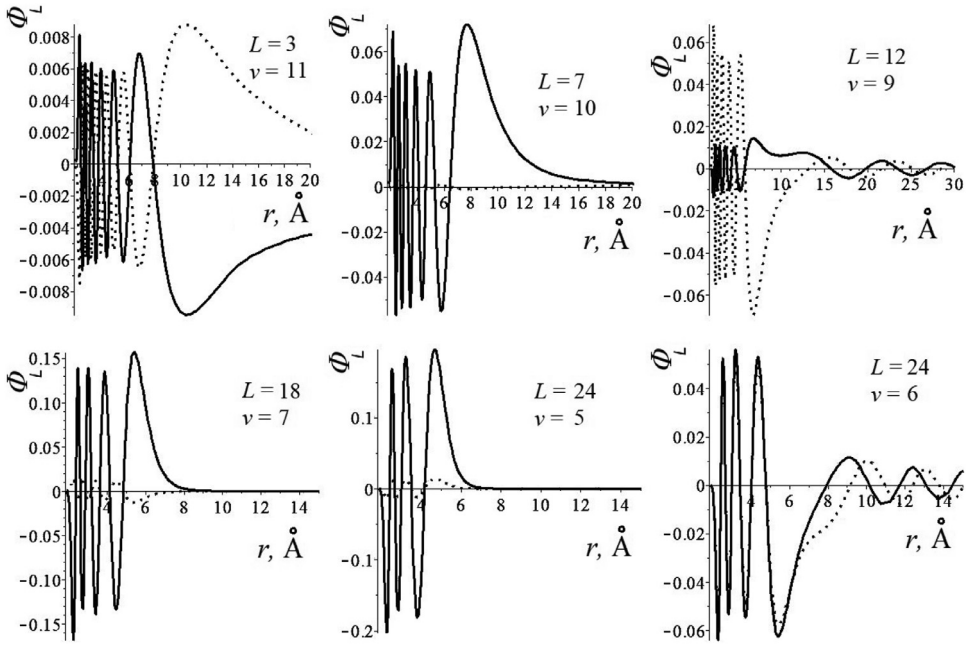

Fig. 3. Plots of real (solid curve) and imaginary (dashed curve) parts of eigenfunctions $\Phi_L \equiv \Phi_{Lv}^M(r)$ of selected metastable states having eigenvalues from the table marked by L =3, 7, 12, 18, 24 and v.

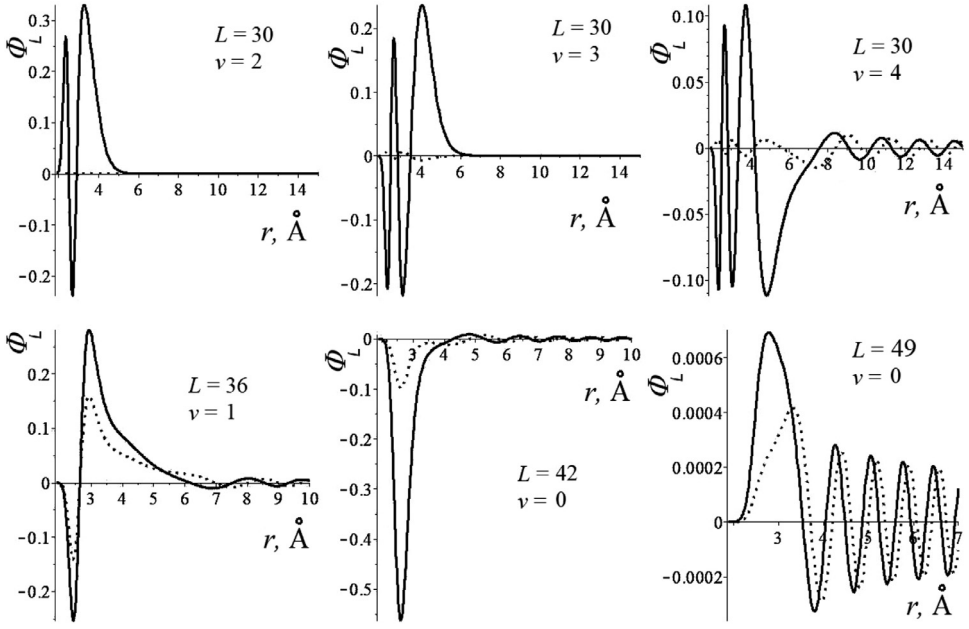

Fig. 4. Plots of real (solid curve) and imaginary (dashed curve) parts of eigenfunctions $\Phi_L \equiv \Phi_{Lv}^M(r)$ of selected metastable states having eigenvalues from the table marked by L =30, 36, 42, 49 and v.

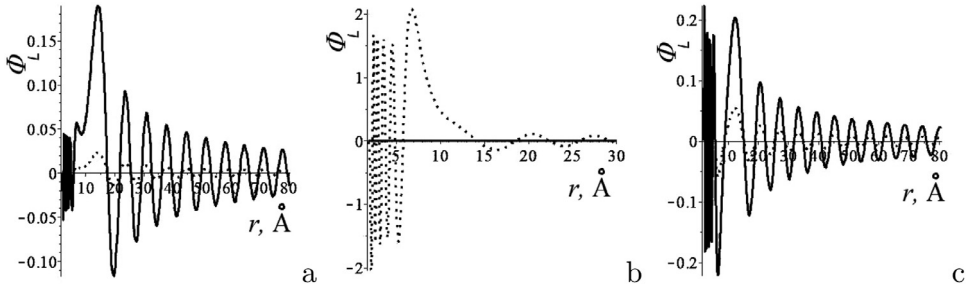

Fig. 5. Plots of the real (solid) and imaginary (dashed) parts of scattering functions $\Phi_L \equiv \Phi_L(r)$ in the vicinity of the resonance energy $E(res) \approx 4.0444958$ cm^{-1} at $L = 12$ (b) and at energies $E = E(res) - 0.5$ cm^{-1} (a) and $E = E(res) + 0.5$ cm^{-1} (c).

Table 5
The rotational-vibrational metastable states $E^M_{Lv} = \Re E^M_{Lv} + \imath \Im E^M_{Lv}$ (in cm^{-1}) of Be_2, where "eps" means that $-10^{-5} < \Im E^M_{Lv} < 0$ (in cm^{-1}). Continuation of Table 4

L	v	MEMO		STO		MEMO		STO	
		$V_L^{\min}$	$V_L^{\max}$	$V_L^{\min}$	$V_L^{\max}$	$\Re E$	$-\Im E$	$\Re E$	$-\Im E$
24	5	−561.68	35.18	−565.28	34.17	11.484	eps	8.853	eps
24	6	−561.68	35.18	−565.28	34.17	32.872	0.169	30.743	0.037
25	4	−531.76	39.58	−534.87	38.36	22.998	eps	20.324	eps
*25	5	−531.76	39.58	−534.87	38.36	40.608	1.156	38.193	0.722
26	4	−500.63	44.18	−503.34	42.90	7.996	eps	4.773	eps
26	5	−500.63	44.18	−503.34	42.90	34.354	1.4e-3	31.670	1.3e-4
27	4	−468.31	49.30	−470.75	47.80	22.032	eps	18.779	eps
27	5	−468.31	49.30	−470.75	47.80	45.187	0.100	42.567	0.034
28	3	−434.78	54.66	−436.96	53.00	6.963	eps	3.009	eps
28	4	−434.78	54.66	−436.96	53.00	35.991	eps	32.731	eps
*28	5	−434.78	54.66	−436.96	53.00	55.158	0.963	52.659	0.817
29	3	−400.25	60.57	−401.96	58.57	23.517	eps	19.452	eps
29	4	−400.25	60.57	−401.96	58.57	49.669	3.0e-4	46.445	5.2e-4
30	2	−364.62	66.91	−401.96	64.70	11.354	eps	7.180	eps
30	3	−364.62	66.91	−365.83	64.70	40.058	eps	35.968	eps
30	4	−364.62	66.91	−365.83	64.70	62.639	0.155	59.548	0.091
31	2	−327.81	73.60	−365.83	71.30	32.621	eps	28.549	eps
31	3	−327.81	73.60	−328.72	71.30	56.534	1.6e-4	52.550	1e-5
*31	4	−327.81	73.60	−328.72	71.30	74.625	1.305	71.651	0.818
32	2	−290.09	80.68	−290.41	78.37	52.660	eps	48.671	eps
32	3	−290.09	80.68	−290.41	78.37	72.662	0.030	68.982	0.013
33	1	−251.21	88.21	−250.90	85.94	15.028	eps	8.238	eps
33	2	−251.21	88.21	−250.90	85.94	71.131	2.4e-4		
33	3	−251.21	88.21	−250.90	85.94	87.630	0.696		
34	1	−211.33	80.42	−210.26	94.04	47.644	eps	40.779	eps
35	1	−170.41	101.47	−168.69	102.73	80.254	eps	73.432	eps
36	1	−128.47	124.02	−126.36	120.39	111.593	0.057	105.388	7.1e-3

Table 6
The rotational-vibrational metastable states $E^M_{Lv} = \Re E^M_{Lv} + \imath \Im E^M_{Lv}$ (in cm^{-1}) of Be_2, where "eps" means that $-10^{-5} < \Im E^M_{Lv} < 0$ (in cm^{-1}). Continuation of Table 5.

L	v	MEMO		STO		MEMO		STO	
		$V_L^{\min}$	$V_L^{\max}$	$V_L^{\min}$	$V_L^{\max}$	$\Re E$	$-\Im E$	$\Re E$	$-\Im E$
37	0	−85.56	147.94	−83.10	144.01	11.780	eps	9.538	eps
37	1	−85.56	147.94	−83.10	144.01	143.263	3.429	135.737	3.656
38	0	−41.66	173.18	−38.98	168.91	53.590	eps	51.2338	eps
*38	1	−41.66	173.18	−38.98	168.91	174.945	4.014	167.103	3.847
39	0	3.20	199.73	6.08	195.12	96.169	eps	93.6727	eps
40	0	48.96	227.57	52.06	222.65	139.466	eps	136.795	eps
41	0	95.70	256.70	98.87	251.52	183.406	8.3e-4	180.520	1.2e-3
42	0	143.28	287.15	146.47	281.76	227.880	0.023	224.726	0.030
43	0	191.72	318.91	194.87	313.39	272.755	0.148	269.267	0.173
44	0	241.02	352.03	244.03	345.95	317.922	0.544	314.016	0.621
45	0	291.13	386.52	293.92	379.25	363.371	1.432	358.964	1.622
46	0	342.01	422.41	344.47	413.44	409.200	3.007	403.499	5.838
47	0	393.59	459.74	395.60	449.11	450.402	6.810	445.144	6.238
*48	0	445.84	498.57	447.31	487.86	499.563	5.439	489.343	7.245
*49	0	498.71	538.92	499.48	528.37	542.927	6.046		
50		552.15	580.82	552.02	570.61				
51		606.00	624.52	604.78	614.64				
52		660.18	670.09	657.53	660.69				
53		714.45	717.43						
54									

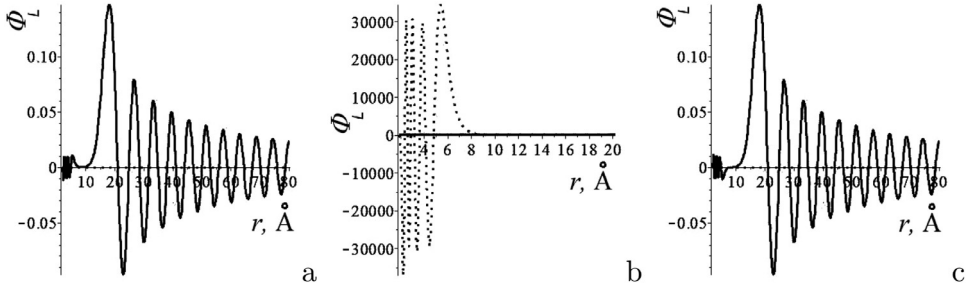

Fig. 6. Plots of the real (solid) and imaginary (dashed) parts of scattering functions $\Phi_L \equiv \Phi_L(r)$ in the vicinity of resonance energy $E(res) \approx 4.78829358850231$ cm^{-1} at $L = 18$ (b) and at energies $E = E(res) - 10^{-3}$ cm^{-1} (a) and $E = E(res) + 10^{-3}$ cm^{-1} (c).

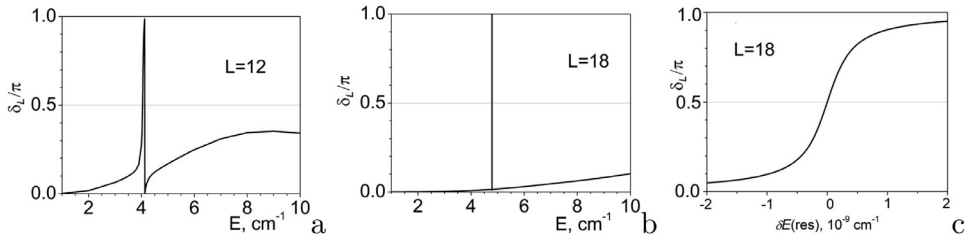

Fig. 7. Phase shifts δ_L vs scattering energy E counted from $E(0)$ at $L = 12$ (a) and $L = 18$ (b). Phase shifts δ at $L = 18$ in the vicinity of resonance energy $E(res)$ (c). Here $\delta E(res) = E - E(res)$.

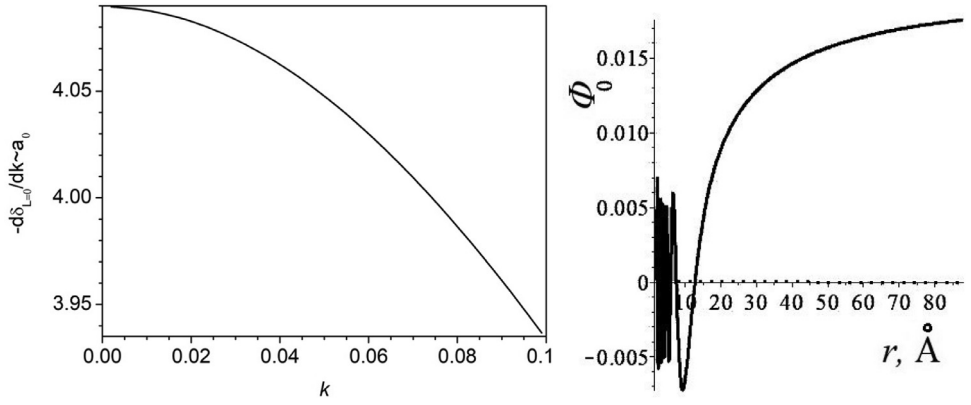

Fig. 8. Estimate of scattering length a_0 in Å vs $k = \sqrt{\mathcal{E}}$ in Å^{-1} and wave function $\Phi_0 \equiv \Phi_0(r)$ at $k = 0.001$Å^{-1}, $L = 0$.

4. Metastable states of the beryllium dimer

The complex eigenenergies $E^M_{Lv} = \Re E^M_{Lv} + \imath \Im E^M_{Lv}$, (in cm^{-1}) of Be_2 rotational-vibrational metastable states, where v is the number of states at fixed value of L, are shown in Tables 4 and 6. Their real parts $\Re E^M_{Lv}$ in comparison with the eigenenergies E_{vL} of vibrational-rotational bound states are displayed in lower panel of Fig. 2b. Note that the real parts of energies $\Re E^M_{Lv}$ of the metastable states marked by an asterisk in Tables 4 and 6 lie above the top $V_L^{\max}$ of the potential barrier $V_L(r)$. The BVP for Eq. (1) was solved by the FEM programs on the above finite element mesh Ω_1 with mixed BVPs, i.e. the Neumann BC at the left point r_1 of the finite interval $r \in [r_1, r^{\max}]$ and the third-type or Robin BC at the right point r_{max} which is calculated using the corresponding asymptotic solution $\Phi^{M(as)}_{Lv}(r)$ in the form of an outgoing wave [22].

The BVP for Eq. (1) was solved using the FEM programs KANTBP 5M on the finite element mesh $\Omega_1 = \{1.90,\ 1.95,\ 2.00,\ 2.07,\ 2.15,\ 2.22,\ 2.30,\ 2.36,\ 2.42,\ 2.50\ (0.1)\ 4\ (\gamma_1)\ 6\ (\gamma_2)\ 14\ (\gamma_3)\ \gamma_4\}$, where $\gamma_1 = \{0.2, L < 44; 0.1\}$, $\gamma_2 = \{0.5, L < 25; 0.25, L < 38; 0.1(6), L < 44; 0.125\}$, $\gamma_3 = 3.1/\sqrt{V^{\max}_{L_9}}$, $L_9 = \max(L, 9)\gamma_4$ is the lowest number of sequence $14 + n\gamma_3$, $n \in \mathcal{N}$ greater than 80, with the Neumann boundary conditions on the boundary point $r = 1.90$ and the Robin boundary condition with logarithmic derivative for $\Phi_L(kr) \equiv \Phi^M_{Lv}(kr)$

$$\frac{d\Phi(kr)}{dr} - R\Phi(kr) = 0,\ R = \frac{1}{\Phi^+_{as}(kr)}\frac{d\Phi^+_{as}(kr)}{dr} = \frac{L}{r} - k\frac{H^{(1)}_{L+3/2}(kr)}{H^{(1)}_{L+1/2}(kr)}, \tag{4}$$

that followed from asymptotic solution for only the outgoing wave $\Phi^+_{as}(kr)$ [22]

$$\Phi^{\pm}_{as}(kr) = \frac{\sqrt{\pi/2}}{\sqrt{r}}H^{(1,2)}_{L+1/2}(kr) = \mp\imath\frac{\exp(\pm\imath(kr - \pi L/2))}{\sqrt{kr}} + O(k^{-3/2}r^{-2}). \tag{5}$$

Here $k \equiv k^M_{Lv} = \sqrt{\mathcal{E}^M_{Lv}} = \sqrt{E^M_{Lv}/s_2}$ in Å^{-1} is the wave number and E^M_{Lv}=$s_2\mathcal{E}^M_{Lv}$ cm^{-1}, $H^{(1,2)}_{L+1/2}(r)$ and $H^{(1,2)}_{L+3/2}(r)$ are Hankel functions [28] ($\frac{d}{dz}H^{(1,2)}_{L+1/2}(z) = (L+1/2)H^{(1,2)}_{L+1/2}(z)/z - H^{(1)}_{L+3/2}(z)$) and $s_2 = 1/0.2672973729$ is the conversion factor from cm^{-1} to Å^{-2}. The potential functions $V_L(r)$ at $L = 3, 7, 8, 11, 12, 14, \ldots, 49$ supported this set of metastable states. These functions are plotted in Fig. 2a at $L = 8, \ldots, 56$ with the step 4.

For $L > 0$ the potential functions at large r decrease proportionally to r^{-2} and at $L \le 38$ have the form of a potential well with a minimum below the dissociation threshold D_0, while at $L > 38$ the potential well has a minimum above the dissociation threshold. The height of the centrifugal barrier increases with increasing L, but its width at the dissociation threshold energy is infinite. With increasing energy, the effective width of the barrier decreases. The number of metastable states δv at $L \le 38$ is determined by the number of positive-energy states in the potential well with the barrier with the height $V_L^{\max}$ taken into account, i.e., in the well with the potential $V^*_L = \{V(r), r < r_{\max}; V_{\max}, r \ge r_{\max}\}$. For small $L < 16$ the barrier height $V_L^{\max}$ counted from the zero energy is smaller than the energy difference between two upper levels of metastable states. This means that even one metastable state can exist not for all values of L. With the growth of L to $L = 33$ the barrier height increases, but the width of the well changes insignificantly. As a result, the number of metastable states increases to three. With further increase in L, when in the interval $r \in (3.5, 6)$ the slope of centrifugal potential exceeds the slope of MEMO potential, the well width rapidly decreases, so that only two states can exist in the well, a bound state and a metastable one at $L = 34, 35, 36$ and two metastable states at $L = 37, 38$. At $L \ge 39$ the potential well minimum turns to be above the dissociation threshold and the effective barrier width, the width and depth of the well decrease. Only one state exists in the well, its width increasing with the growth of L. At $L > 49$ there are no energy levels in the well, and at $L > 54$ the potential well disappears.

As can be seen from Tables 2, 4 and 6 and Figs. 3–4, the eigenfunctions of metastable states with complex energy values for a fixed value of the orbital momentum L have an increasing number of nodes localized inside the potential well. Beginning from each lower state above the dissociation threshold, they have one node more than the last bound state with real energy under the dissociation threshold ($E = 0$) with the same value of the orbital momentum L. Thus, there is a continuation of the *upper and lower estimates* of the real energy eigenvalues $E_{Lv} = \Re E_{Lv}$ to the complex plane $E^M_{Lv} = \Re E^M_{Lv} + \imath \Im E^M_{Lv}$, labelled by the number of nodes of eigenfunctions localized inside the potential well, for each value of the orbital moment L.

5. Scattering states of the beryllium dimer

The scattering problem for Eq. (1) at real-valued $E > 0$ in cm^{-1} was solved using the FEM programs KANTBP 5M on the finite element mesh $\Omega_1 = \{1.90,\ 1.95,\ 2.00,\ 2.07,\ 2.15,\ 2.22,\ 2.30,\ 2.36,\ 2.42,\ 2.50\ (0.1)\ 4\ (\gamma_1)\ 6(\gamma_2)\ 14\ (\gamma_3)\ \gamma_4\}$, where $\gamma_1 = \{0.2, E < 360; 0.1\}$, $\gamma_2 = \{0.5, E < 35; 0.25, E < 148; 0.1(6), E < 320; 0.125\}$, $\gamma_3 = 2.9/\sqrt{E}$, γ_4 is the lowest number of sequence $14 + n\gamma_3$, $n \in \mathcal{N}$ greater than 80. The eigenfunctions $\Phi_L(kr)$ of the scattering states are subjected the Neumann boundary conditions (BCs) on the boundary point $r = r_{\min} = 1.90$ and the Robin boundary condition formulated by the following relations:

$$\frac{d\Phi_L(kr)}{dr} = \frac{d\Phi^L_{as}(kr)}{dr}, \quad \Phi_L(kr) = \Phi^L_{as}(kr), \tag{6}$$

at $r = r_{\max}$ using the asymptotic form "incident wave + outgoing wave" [28]

$$\Phi^L_{as}(r) = \frac{1}{2}(\Phi^-_{as}(kr) + \Phi^+_{as}(kr)S_L(E)). \tag{7}$$

Here $S_L(E) = \exp(2\imath\delta_L(E))$ is the partial scattering matrix, and $\Phi^\pm_{as}(kr)$ are given by formula (4) at real-valued $k = \sqrt{\mathcal{E}} > 0$ in $Å^{-1}$.

Plots of the real (solid) and imaginary (dashed) parts of scattering functions in the vicinity of the resonance energy for the narrow resonance at $L = 12$ and very narrow resonance at $L = 18$ are shown in Figs. 5 and 6. One can see that the resonant scattering functions are localized in the potential well, which is no longer observed with a minor change in the energy of the incident wave. As can be seen from Tables 4 and 6, the energies of resonant states coincide with the real parts of the energies of metastable states. In Fig. 7 the phase shifts δ vs the scattering energy E are shown, as expected, the phase shifts take the value $\delta = \pi/2$ for resonant energies and change rapidly in their vicinity. For rough estimation of scattering length a_S of the scattering state at $k \to 0$ one can apply the formula

$$a_0 = -\lim_{k\to 0}\frac{\tan\delta_0(k)}{k} \approx -\frac{d\delta_0(k)}{dk}\Big|_{k\to 0} \approx -\frac{\delta_0(k_{i+1}) - \delta_0(k_{i-1})}{k_{i+1} - k_{i-1}}\Big|_{k_i\to 0},$$

where $k^{-1} = \sqrt{1/\mathcal{E}}$ in Åand $\mathcal{E}$ in $Å^{-2}$ are accepted in our calculations. The calculated plot $-\frac{d\delta_0(k)}{dk} \approx a_0$ presented in Fig. 8 gives us an estimate for $a_0 \approx 3.348$ Å. For example, a plot of the corresponding wave function is shown at $k = 0.001Å^{-1}$.

6. Conclusion

The efficacy of the applied approach and programs is demonstrated by the *upper and lower estimates* of twelve eigenenergies of the vibrational bound states of the beryllium dimer with the required accuracy in comparison with those known from literature, as well as the vibrational-rotational spectrum bound states and rotational-vibrational spectrum of narrow-band metastable states with complex valued eigenenergies.

We believe that these results can serve as a guide for future high-precision laser spectroscopy of weakly-bound, metastable and scattering states of the beryllium dimer. Laser spectroscopy of such objects offers unique opportunities for clarifying the nature of electron correlation bonding in molecules that could not exist in the standard chemical bond theory based on the Hartree-Fock self-consistent field approximation.

The presented approach and KANTBP 5M program [19] provide a useful tool for further study of approximations of the tabulated potential function in a finite interval and its extension beyond this interval using asymptotic expansions and its matching via interpolation Hermite polynomials, and modeling calculations of the weakly bound states with eigenenergies close to the dissociation threshold and processes of near-surface diffusion of diatomic molecules [12].

Declaration of Competing Interest

The authors declare that they have no known competing financial interests or personal relationships that could have appeared to influence the work reported in this paper.

CRediT authorship contribution statement

V.L. Derbov: Conceptualization, Writing - review & editing. **G. Chuluunbaatar:** Software, Visualization. **A.A. Gusev:** Software, Visualization. **O. Chuluunbaatar:** Software. **S.I. Vinitsky:** Conceptualization, Writing - original draft. **A. Góźdź:** Methodology. **P.M. Krassovitskiy:** Software. **I. Filikhin:** Validation. **A.V. Mitin:** Supervision.

Acknowledgements

The work was partially supported by the RFBR and MECSS, project number 20-51-44001, the Ministry of Education and Science of the Russian Federation, project number 075-10-2020-117, the Foundation of Science and Technology of Mongolia, project number SST 18/2018, the Bogoliubov-Infeld program, the Hulubei-Meshcheryakov program, by the RUDN University Strategic Academic Leadership Program and grant of Plenipotentiary of the Republic of Kazakhstan in JINR.

Supplementary material

The following file is available free of charge. supp.pdf: contains the MAPLE and FORTRAN programs of approximation of the MEMO [4] and STO [6] potential functions $V_L(r)$ and example at $L = 0$.

Supplementary material associated with this article can be found, in the online version, at 10.1016/j.jqsrt.2021.107529.

References

[1] Patkowski K, Špirko V, Szalewicz K. On the elusive twelfth vibrational state of beryllium dimer. Science 2009;326(5958):1382–4. doi:10.1126/science.1181017.
[2] Mitin AV. Ab initio calculations of weakly bonded He2 and Be2 molecules by MRCI method with pseudo-natural molecular orbitals. Int J Quantum Chem 2011;111(11):2560–7. doi:10.1002/qua.22691.
[3] Koput J. The ground-state potential energy function of a beryllium dimer determined using the single-reference coupled-cluster approach. PCCP 2011;13(45):20311–17. doi:10.1039/c1cp22417d.
[4] Mitin AV. Unusual chemical bonding in the beryllium dimer and its twelve vibrational levels. Chem Phys Lett 2017;682:30–3. doi:10.1016/j.cplett.2017.05.071.
[5] Meshkov VV, Stolyarov AV, Heaven MC, Haugen C, LeRoy RJ. Direct potential-fit analysis yield improved empirical potentials for the ground $x^1\sigma_g^+$ state of Be_2. J Chem Phys 2014;140(6):064315. doi:10.1063/1.4864355.
[6] Lesiuk M, Przybytek M, Balcerzak JG, Musiał M, Moszynski R. Ab initio potential energy curve for the ground state of beryllium dimer. J Chem Theory Comput 2019;15:2470–80. doi:10.1021/acs.jctc.8b00845.
[7] Merritt JM, Bondybey VE, Heaven MC. Beryllium dimer – caught in the act of bonding. Science 2009;324(5934):1548–51. doi:10.1126/science.1174326.

[8] Gusev A, Chuluunbaatar O, Vinitsky S, Derbov VL, Gozdz A, Krassovitskiy PM, Filikhin I, Mitin AV, Hai LL, Lua TT. On rotational-vibrational spectrum of diatomic beryllium molecule. In: Proceedings of SPIE, vol. 11066; 2019. p. 1106619. doi:10.1117/12.2518409.
[9] Porsev SG, Derevianko A. High-accuracy calculations of dipole, quadrupole, and octupole electric dynamic polarizabilities and van der Waals coefficients C_6, C_8, and C_{10} for alkaline-earth dimers. J Exp Theor Phys 2006;102:195–205. doi:10.1134/S1063776106020014.
[10] Sheng XW, Kuang XY, Li P, Tang KT. Analyzing and modeling the interaction potential of the ground-state beryllium dimer. Phys Rev A 2013;88(2):022517. doi:10.1103/PhysRevA.88.022517.
[11] Derbov VL, Chuluunbaatar G, Gusev AA, Chuluunbaatar O, Vinitsky SI, Góźdź A, Krassovitskiy PM, Mitin AV. On calculations of metastable and Rydberg states of diatomic beryllium molecule and antiprotonic helium atom. In: Proc. of SPIE, vol. 11458; 2020. p. 114580. doi:10.1117/12.2565816.
[12] Gusev AA, Vinitsky SI, Chuluunbaatar O, Góźdź A, Derbov VL, Krassovitskiy PM. Adiabatic representation for atomic dimers and trimers in collinear configuration. Phys Atomic Nuclei 2018;81:945–70. doi:10.1134/S1063778818060169.
[13] Walsh KA. Beryllium chemistry and processing. ASM International, Materials Park, OH, USA; 2009.
[14] Allouche A, Linsmeier C. Quantum study of tungsten interaction with beryllium (0001). J Phys 2008;117:012002. doi:10.1088/1742-6596/117/1/012002.
[15] Chuluunbaatar O, Gusev AA, Vinitsky SI, Abrashkevich AG. ODPEVP: a program for computing eigenvalues and eigenfunctions and their first derivatives with respect to the parameter of the parametric self-adjoined Sturm-Liouville problem. Comput Phys Commun 2009;181:1358–75. doi:10.1016/j.cpc.2009.04.017.
[16] Chuluunbaatar O, Gusev AA, Abrashkevich AG, Amaya-Tapia A, Kaschiev MS, Larsen SY, Vinitsky SI. KANTBP: a program for computing energy levels, reaction matrix and radial wave functions in the coupled-channel hyperspherical adiabatic approach. Comput Phys Commun 2007;177:649–75. doi:10.1016/j.cpc.2007.05.016.
[17] Chuluunbaatar O, Gusev AA, Vinitsky SI, Abrashkevich AG. KANTBP 2.0: new version of a program for computing energy levels, reaction matrix and radial wave functions in the coupled-channel hyperspherical adiabatic approach. Comput Phys Commun 2008;179:685–93. doi:10.1016/j.cpc.2008.06.005.
[18] Gusev AA, Chuluunbaatar O, Vinitsky SI, Abrashkevich AG. KANTBP 3.0: new version of a program for computing energy levels, reflection and transmission matrices, and corresponding wave functions in the coupled-channel adiabatic approach. Comput Phys Commun 2014;185:3341–3. doi:10.1016/j.cpc.2014.08.002.
[19] Gusev A, Vinitsky S, Gerdt V, Chuluunbaatar O, Chuluunbaatar G, Hai LL, Zima E. A maple implementation of the finite element method for solving boundary problems of the systems of ordinary second order differential equations. In: Talk in MAPLE 2020 conference; 2020. https://www.maplesoft.com/mapleconference/MapleConference2020-LiveQA.pdf
[20] Gusev AA, Chuluunbaatar O, Vinitsky SI, Hai LL. KANTBP 4M — program for solving boundary problems of the self-adjoint system of ordinary second order differential equations. JINRLIB; 2015. http://wwwinfo.jinr.ru/programs/jinrlib/kantbp4m
[21] Gusev AA, Chuluunbaatar O, Vinitsky SI, Derbov VL, Gozdz A, Hai LL, Rostovtsev VA. Symbolic-numerical solution of boundary-value problems with self-adjoint second-order differential equation using the finite element method with interpolation hermite polynomials. Lect Notes Comput Sci 2014;8660:138–54. doi:10.1007/978-3-319-10515-4_11.
[22] Gusev AA, Hai LL, Chuluunbaatar O, Ulziibayar V, Vinitsky SI, Derbov VL, Gozdz A, Rostovtsev VA. Symbolic-numeric solution of boundary-value problems for the schrodinger equation using the finite element method: scattering problem and resonance states. Lect Notes Comput Sci 2015;9301:182–97. doi:10.1007/978-3-319-24021-3_14.
[23] Atomic spectroscopy databases. https://www.nist.gov/pml/atomic-spectroscopy-databases.
[24] Douglas M, Kroll NM. Quantum electrodynamical corrections to the fine structure of helium. Ann Phys 1974;82(1):89–155. doi:10.1016/0003-4916(74)90333-9.
[25] Hess BA. Applicability of the no-pair equation with free-particle projection operators to atomic and molecular structure calculations. Phys Rev A 1985;32(2):756–63. doi:10.1103/PhysRevA.32.756.
[26] Hess BA. Relativistic electronic-structure calculations employing a two-component no-pair formalism with external-field projection operators. Phys Rev A 1986;33(6):3742–8. doi:10.1103/PhysRevA.33.3742.
[27] Gdanitz RJ. Accurately solving the electronic Schrödinger equation of atoms and molecules by extrapolating to the basis set limit. I. The helium dimer (He2). J Chem Phys 2000;113(13):5145–53. doi:10.1063/1.1290001.
[28] Goldberger ML, Watson KM. Collision theory. NY: John Wiley & Sons, Inc; 1964.